

Key conclusions of the first international urban land surface model comparison project

Article

Accepted Version

Best, M. J. and Grimmond, C. S. B. ORCID:
<https://orcid.org/0000-0002-3166-9415> (2015) Key conclusions of the first international urban land surface model comparison project. *Bulletin of the American Meteorological Society*, 96 (5). pp. 805-819. ISSN 1520-0477 doi: 10.1175/BAMS-D-14-00122.1 Available at <https://centaur.reading.ac.uk/37718/>

It is advisable to refer to the publisher's version if you intend to cite from the work. See [Guidance on citing](#).

Published version at: <http://dx.doi.org/10.1175/BAMS-D-14-00122.1>

To link to this article DOI: <http://dx.doi.org/10.1175/BAMS-D-14-00122.1>

Publisher: American Meteorological Society

All outputs in CentAUR are protected by Intellectual Property Rights law, including copyright law. Copyright and IPR is retained by the creators or other copyright holders. Terms and conditions for use of this material are defined in the [End User Agreement](#).

www.reading.ac.uk/centaur

CentAUR

Central Archive at the University of Reading

Reading's research outputs online

1 **Key conclusions of the first international urban land surface model comparison**
2 **project**

3

4 M.J. Best, C.S.B. Grimmond

5

6

7 AFFILIATIONS: Best – Met Office, Exeter, UK, and King’s College London,
8 London, UK; Grimmond – University of Reading, Reading, UK

9

10 CORRESPONDING AUTHOR: Martin J. Best, Met Office, FitzRoy Road, Exeter,
11 EX1 3PB, UK.

12 E-mail: martin.best@metoffice.gov.uk

13

14 **ABSTRACT:** The first international urban land surface model comparison was
15 designed to identify three aspects of the urban surface-atmosphere interactions: (1) the
16 dominant physical processes, (2) the level of complexity required to model these, and
17 (3) the parameter requirements for such a model. Offline simulations from 32 land
18 surface schemes, with varying complexity, contributed to the comparison. Model
19 results were analysed within a framework of physical classifications and over four
20 stages. The results show that the following are important urban processes; (i) multiple
21 reflections of shortwave radiation within street canyons, (ii) reduction in the amount
22 of visible sky from within the canyon, which impacts on the net long-wave radiation,
23 (iii) the contrast in surface temperatures between building roofs and street canyons,
24 and (iv) evaporation from vegetation. Models that use an appropriate bulk albedo
25 based on multiple solar reflections, represent building roof surfaces separately from
26 street canyons and include a representation of vegetation demonstrate more skill, but
27 require parameter information on the albedo, height of the buildings relative to the
28 width of the streets (height to width ratio), the fraction of building roofs compared to
29 street canyons from a plan view (plan area fraction) and the fraction of the surface that
30 is vegetated. These results, whilst based on a single site and less than 18 months of
31 data, have implications for the future design of urban land surface models, the data
32 that need to be measured in urban observational campaigns, and what needs to be
33 included in initiatives for regional and global parameter databases.

34

35 **Capsule Summary**

36 The conclusions from the first international urban land surface model comparison
37 project have implications for future models, observations and parameter databases,
38 that extend beyond the urban modelling community

39

40 **1. Introduction**

41 Urban areas are often warmer than their surrounding rural environments, referred to as
42 the urban heat island (UHI). This urban warming has numerous effects, including the
43 initiation of convective storms (e.g., *Bornstein and Lin, 2000*), altering pollution
44 dispersion by adapting mixing through changes to atmospheric boundary layer
45 structure (e.g., *Sarrat et al., 2006, Luhar et al., 2014*), impacts on the production and
46 mixing of ozone (e.g., *Chaxel and Chollet, 2009, Ryu et al., 2013*), enhanced energy
47 demand for summer-time cooling through air conditioning (e.g., *Radhi and Sharples,*
48 *2013, Li et al., 2014*), impacts on urban ecology (e.g., *Pickett et al., 2008, Francis and*
49 *Chadwick, 2013*) and increased mortality rates during heat waves (e.g., *Laaidi et al.,*
50 *2012, Herbst et al., 2014, Saha et al., 2014*). As such, it is important to be able to
51 accurately forecast urban warming and other meteorological variables for cities where
52 the majority of the World's population now lives.

53

54 Predictions of future climate suggest additional warming in urban environments
55 (*McCarthy et al., 2010, Oleson et al., 2011*). Indeed, the Inter-Governmental Panel on
56 Climate Change (IPCC) Working Group 1 Fifth Assessment Report (*IPCC, 2013*)
57 included at least one model that explicitly included an urban representation, and this
58 number is likely to increase in the future as the resolution of these climate models
59 increases to the extent that some urban areas are resolved. For future design of

60 buildings and planning of cities, it is important that the dominant processes that lead
61 to urban warming effects are considered. This requires the development of models
62 that can represent the most important features of the urban heat island be used for
63 reliable predictions.

64

65 The urban heat island results from differences in surface energy exchanges between
66 the urban environment and its surrounding rural area. Thus, understanding these
67 differences is needed to interpret the urban heat island. The differences in urban
68 surface energy exchanges arise through a number of processes. The geometry of a
69 street canyon will increase the incoming solar radiation and long-wave radiation that
70 are absorbed, due to multiple reflections and re-radiated from the 3-dimensional
71 structures. The orientation of street canyons and the elevation of the sun will impact
72 the reflected solar radiation, as a consequence of the depth to which the direct
73 sunshine can penetrate into the canyon. The reduced availability of water at the urban
74 surface, compared to natural vegetated or bare soil surfaces, means more of the
75 incoming solar radiation is transformed into heat rather than a flux of moisture into
76 the atmosphere. However, a larger proportion of this energy for heating is held within
77 the fabric of the buildings given the large thermal inertia of the materials, resulting in
78 changes in the diurnal cycle of urban temperatures. Moreover, an additional source of
79 heating within the urban areas comes from human activities such as transport, the
80 internal heating of the buildings and the metabolic rates of the people themselves
81 (e.g., Sailor and Lu, 2004).

82

83 All of these processes contribute to the differences in the energy balance between
84 urban and rural surfaces, but it is difficult to identify which are the dominant

85 processes just from observations as the processes cannot be separated because of the
86 complex nature of the environment. As such, the best way to study these processes
87 individually is by using urban land surface models (ULSMs) that have been
88 developed for weather and climate applications, i.e., exchange surface fluxes with an
89 atmospheric model. There are a number of such ULSMs that vary considerably in
90 their complexity (e.g., *Kusaka et al.*, 2001, *Fortuniak*, 2003, *Krayenhoff and Voogt*,
91 2007, *Hamdi and Masson*, 2008, *Lee and Park*, 2008, *Oleson et al.*, 2008a). Although
92 newer models often include more complex features than previous models, without
93 knowing the dominant processes and controls, it is difficult to quantify the impact of
94 each new feature.

95

96 The first urban land surface model comparison was designed to objectively assess and
97 compare the performance of a range of ULSMs for a single observational site. It
98 attempted to identify the dominant physical processes that need to be represented in
99 ULSMs by comparing models of varying complexity (Table 1). These models ranged
100 from simple bulk representations of the surface that have been applied to atmospheric
101 models for over a decade, representations of the facets of a street canyon (i.e., roofs,
102 walls and road) that have been used in weather and climate models, through to more
103 recently developed schemes that consider a complete energy balance at various levels
104 within the urban canyon that have been applied to stand alone single point studies.
105 Figure 1 shows a conceptual representation of the surface energy balance for these
106 models of varying complexity. Whilst the scale that these models typically represent
107 is larger than the size of the elements within a street canyon, a common feature is the
108 ability to predict the exchange of fluxes between the urban surface and the atmosphere
109 above it, i.e., the net all-wave radiation (Q^*), turbulent sensible (Q_H) and latent heat

110 (Q_E) fluxes, as measured from flux towers in numerous urban observational
111 campaigns.

112 The aim of the urban model comparison was to consider:

113 (1) What are the dominant physical processes in the urban environment?

114 (2) What is the level of complexity required for an ULSM to be fit for purpose?

115 (3) What are the parameter requirements for such a model?

116 Here we present an analysis of the model comparison results to address these
117 questions.

118

119 **2 Model Comparison design**

120 **2.1 Observational data**

121 The criteria for selecting the evaluation dataset were; first it had not been used to
122 evaluate any ULSMs previously, and second it needed to cover an annual cycle to
123 allow assessment for different seasons. Model evaluation studies often result in the
124 development and optimisation of a model in order to obtain better representation of
125 the assessed metrics. Hence, using a dataset previously used by one or a sub-set of the
126 models to be evaluated would not enable a clean/independent objective assessment for
127 all of the models.

128

129 The dataset for a suburb of Melbourne (Preston) (*Coutts et al.*, 2007a, 2007b) that had
130 observations from 13 August 2003 to 13 November 2004 was selected. The
131 moderately developed, low-density housing area is classified by *Coutts et al.* (2007b)
132 as an Urban Climate Zone (UCZ) 5 (*Oke*, 2006), Local Climate Zone (LCZ) 6
133 (*Stewart and Oke*, 2012) or *Loridan and Grimmond* (2012) Urban Zone for Energy
134 exchange (UZE) medium density. The description of UCZ 5 is “medium

135 development, low density suburban with 1 or 2 storey houses, e.g., suburban housing”
136 (*Oke*, 2006), and as such the site is typical of suburban areas found in North America,
137 Europe and Australasia. The area has mean building height-to-width ratio of 0.42 and
138 mean wall-to-plan ratio of 0.4 (*Coutts et al.*, 2007b). The surface is dominated by
139 impervious cover (44.5% buildings, 4.5% concrete and 13% roads), with a pervious
140 cover of 38% (15% grass, 22.5% other vegetation and 0.5% bare ground or pools)
141 (*Coutts et al.*, 2007a).

142

143 The methods used to obtain the observed fluxes applied to our current analysis are
144 given in Table 2, with details (e.g., data processing) presented in the original
145 observation papers (*Coutts et al.*, 2007a, 2007b). In addition, the initial model
146 comparison results papers (*Grimmond et al.*, 2011, *Best and Grimmond*, 2013, 2014)
147 provide the site parameters. A continuous gap-filled atmospheric forcing dataset (474
148 days) to run the models was created for this study (see *Grimmond et al.*, 2011). To
149 evaluate the modelled fluxes (sensible heat flux, latent heat flux, net all-wave
150 radiative flux and net storage heat flux (ΔQ_s)) 30 min periods are used when no
151 observed fluxes are missing to allow consistent analysis between the fluxes (N=8865
152 or 38.9% of the full period).

153

154 **2.2 Data analysis**

155 To permit the research questions posed above to be considered, information about the
156 observational site was released to the modelling groups in stages. This enabled
157 analysis of the importance of the different types of information to model performance
158 through assessment of the change in model skill between the stages. The stages (Table
159 3), designed to correlate with ease of access to information for all cities globally,

160 involved release of (*Grimmond et al.*, 2011):

161 *Stage 1: Atmospheric forcing data:* (Table 3), typically provided by an atmospheric
162 model.

163 *Stage 2: Vegetation and built fraction:* two dimensional plan area characteristics of
164 the site. These can be determined from land cover datasets derived from satellite data.

165 *Stage 3: Morphology:* three dimensional characteristics of the site (Table 3.). These
166 can be interpreted from LiDAR (e.g., *Goodwin et al.*, 2009, *Lindberg and Grimmond*,
167 2011), aerial photographs (e.g., *Ellefsen*, 1990/1991), detailed satellite imagery (e.g.,
168 *Brunner et al.*, 2010), or simple empirical relations (e.g., *Bohnenstengel et al.*, 2011).

169 *Stage 4: Building material parameters* (Table 3): only obtainable from local
170 knowledge of the materials used in the construction of the buildings.

171 *Stage 5: Observed fluxes:* to allow parameter optimisation studies. Only a few groups
172 completed this stage, so these results are not presented here.

173

174 The results from 24 modelling groups are analysed, involving 21 independent models
175 (Table 1). Alternative versions of the same model were run by the same or
176 independent modelling groups, which resulted in 32 sets of model simulations being
177 submitted for all of the four stages (see full list in *Grimmond et al.*, 2011). Each group
178 completed a survey indicating the level of complexity used for various physical
179 processes within their models. From the latter, categories of physical processes were
180 established, with classes that cover the range of complexities (*Grimmond et al.*, 2010,
181 2011). These categories were chosen to investigate the importance of various physical
182 processes that could contribute to differences in the surface energy balance between
183 the urban and rural environments. Thus every model is assigned to a class in each
184 category based on the survey information. In this study, the complexity category

185 (Grimmond et al., 2011) is not considered as the focus is to separate the specific
186 physical processes. The categories, with the number of models in each class are
187 shown in Table 4.

188

189 Comparing the mean behaviour of the models in each of the classes as a reference
190 provides a method to determine the level of complexity that gives the best
191 performance for each category. These data are analysed to address the second research
192 question, where “fit for purpose” in this study is defined as being able to accurately
193 represent the energy exchange between the urban surface and the atmosphere (i.e., the
194 net all-wave radiation, turbulent sensible and latent heat fluxes).

195

196 Furthermore, by assessing the performance of the models across the categories for all
197 classes, it is possible to identify the physical processes that have the largest impact on
198 the performance of the models, hence identifying the dominant physical processes and
199 addressing the first research question.

200

201 **2.3 Methodology**

202 Initial results from the urban model comparison (Grimmond et al., 2011) ranked the
203 models and assessed the performance of the various classes within the categories
204 using standard statistical measures. Here an alternative approach to assess the models’
205 performance is used, that considers the percentage of the models’ data values that are
206 within observational error (E_{obs}). This gives a measure between zero (no values within
207 observational errors) and 100% (all values within observational errors, i.e., a ‘perfect’
208 model). Although this type of analysis is not strictly benchmarking, as each model is
209 not being compared to an *a priori* metric, it could be considered as being closer to the

210 benchmarking ethos as having all data points within observational errors would be a
 211 stringent metric.
 212
 213 The observational error estimates used in this analysis are for day-time fluxes based
 214 on a percentage of the observed fluxes, as suggested by *Hollinger and Richardson*
 215 (2005): net all-wave radiation flux 5%, turbulent sensible heat flux 10%, latent heat
 216 flux 8%, and upward components of both shortwave and long-wave radiation fluxes
 217 10%. As the net storage heat flux in the observational dataset is determined as the
 218 residual of the surface energy balance, its observational error is assumed to be the sum
 219 of the errors for the other terms (i.e., Q^* , Q_H and Q_E), giving 23%. The night-time
 220 error estimates are assumed to be double the day-time error estimates for each of the
 221 fluxes. The absolute magnitude of fluxes during this period are typically small (order
 222 of (10) W m^{-2}), hence changes in the percentage of the observed flux used as the error
 223 estimates are likely to be within the reporting resolution (e.g. order of (1) W m^{-2}) of
 224 the observations (especially the turbulent fluxes). Whilst these error estimates may be
 225 indicative rather than the actual values, the results would not substantially change the
 226 analysis presented.

227
 228 The analysis was undertaken for each model (k) in each class (j) within each category
 229 (i) (Table 4), for each flux, over each stage within the comparison, and separately for
 230 day-time and night-time. From this the percentage of data within observational error
 231 ($E_{obs,i,j}$) was determined:

$$232 \quad E_{obs,i,j} = \frac{\sum_{k=1}^{n_{ij}} M_k}{n_{ij}T} \times 100\% \quad (1)$$

233 where M is the number of points within observational error for model (k), n is the

234 number of models and T is the number of day-time or night-time points in the time
235 series as appropriate.

236

237 **3. Results**

238 Application of eqn. 1 to the sensible, latent and net storage heat fluxes, for each class
239 and category, at Stage 1 and Stage 4 (Table 3) are shown in Figure 2. The results
240 could range between 0% (i.e., no model data points within the observations errors) to
241 100% (i.e., all model data points within observational errors). The relative changes
242 between the stages are also shown in Figure 2, i.e., for stage (s) the change relative to
243 the previous stage ($s-1$) given by:

$$244 \quad E_{obs,ij}^s / E_{obs,ij}^{s-1} \quad (2)$$

245 Assessment of “between stages performance” allows an emphasis of the common
246 results across all of the classes and categories. It is scaled between 0% and 100%,
247 with 50% corresponding to no change between the stages (Figure 2).

248

249 Generally the results of the analysis, consistent with *Grimmond et al.* (2011), show
250 that the skill to model latent heat fluxes is improved between stages 1 and 2. Knowing
251 the plan area vegetation fraction (provided in Stage 2) is important for modelling the
252 latent heat flux. No other stages show a general increase in model performance across
253 the classes and categories for the fluxes shown in Figure 2. For the radiation fluxes
254 (Fig. 3), the largest changes evident between Stages 3 and 4 are for the reflected
255 shortwave radiation flux and are due to the specification of the bulk albedo at the site
256 (i.e., the ratio of the reflected outgoing shortwave radiation flux from the whole urban
257 surface to the incoming shortwave radiation flux, information released at Stage 4).
258 This is also consistent with the conclusions from *Grimmond et al.* (2011).

259

260 Model performance for the outgoing long-wave radiation flux has its largest changes
261 at night-time between Stages 3 and 4 (when the 3-d site morphological information
262 (Table 3) were made available, Fig. 3). This enhanced performance at night could be
263 related to improved estimates of the sky view factor which influences radiative
264 trapping, and/or from improved estimates of the difference in nocturnal surface
265 temperatures between building roofs and those of the roads and walls of the urban
266 canyons. Improved performance is not detected in the day-time outgoing long-wave
267 radiation flux (Fig. 3), probably because of the dominance of shortwave radiation at
268 this time. These results were not identified in *Grimmond et al. (2011)* as there was no
269 separate analysis for day-time and night-time.

270

271 It is evident from Figures 2 and 3 that the performance of the models for each of the
272 fluxes does not improve consistently for each stage, as might be expected. This
273 suggests that the models are not able to correctly make use of all of the information
274 that is provided at each of the stages and hence the design of the models, and the use
275 of their specific parameters, is not necessarily correct. This is discussed further in
276 *Grimmond et al. (2011)*.

277

278 Each model is assigned to one class for every category (Table 4). This means that a
279 model with particularly good (or poor) performance will influence the results for its
280 class in each of the categories. The implications of this are that it is not possible to
281 ensure that the good performance from a particular class within one category is not
282 actually resulting from the results of a class from a different category. This potential
283 contamination of results by categories inhibits the analysis of the dominant physical

284 processes and the suitability of the models. Both the analysis presented in *Grimmond*
 285 *et al.* (2011) and that in Figures 2 and 3 have this limitation, hence we will not
 286 consider further any results in Figures 2 and 3 for any specific class or category.
 287 Alternatively, to address this issue of cross-contamination, we repeat the complete
 288 analysis using eqn. 1 separately for each category (c), but only considering the subset
 289 of models from class (a). Hence for each class (j) in category (i) for the analysis of
 290 eqn. 1, the models used are those that are in both class (a) of category (c) and class (j)
 291 of category (i), of which there are $n_\alpha = n_{ca} \cap n_{ij}$, thus:

$$292 \quad E_{obs,caij} = \frac{\sum_{k=1}^{n_\alpha} M_k}{n_\alpha T} \times 100\% \quad (3)$$

293 This gives the equivalent of 26 versions of Figures 2 and 3 (one for each class in each
 294 category); although for a given subset of models it is inevitable that some classes will
 295 not have any members and hence have no data. We then apply the following equation
 296 for each of the stages to determine which of the original class of models has the best
 297 performance:

$$298 \quad P_{ca} = \frac{\sum N_m}{N_{tot} - (\sum N_{nd}) - 1} \times 100\% \quad (4)$$

299 where P_{ca} is the percentage of classes in the analysis that are improved from just the
 300 subset of models (compared to the analysis with the full set of models),

$$301 \quad N_m = \sum_{k=1}^{N_{tot}} \begin{cases} 1 & \text{if } E_{obs,caij} > E_{obs,ij} \\ 0 & \text{otherwise} \end{cases} \quad (5)$$

302 is the number of classes that are improved in the analysis, N_{tot} is the total number of
 303 classes ($\sum ij = 26$) and

$$304 \quad N_{nd} = \sum_{k=1}^{N_{tot}} \begin{cases} 1 & \text{if } n_{ca} \cap n_{ij} = 0 \\ 0 & \text{otherwise} \end{cases} \quad (6)$$

305 is the number of classes with no data.

306

307 Hence values of P_{ca} close to 100% relate to nearly all classes in all categories being

308 improved from the physical process represented in class (a) of category (c). This

309 indicates that this process and its representation are important to model performance.

310 Whereas values close to 0% relate to almost all classes in all categories being

311 degraded, suggesting that the representation of the physical process is detrimental to

312 model performance. Values around 50% have a similar number of classes that are

313 improved and degraded, suggesting that the representation of the physical process has

314 little impact on model performance. Hence the conclusions that can be drawn from

315 this analysis are more robust than those of Figures 2 and 3, and the previous study of

316 *Grimmond et al. (2011)*.

317

318 For example, with models that have an infinite number of reflections (category R,

319 class i), the median of the results over the stages give a value of 88% for the night-

320 time net storage heat flux (Fig. 4). This results from 14 of the 16 possible classes

321 containing data being improved when considering only these models, demonstrating

322 that this is important for predicting this flux. However, models that have multiple

323 reflections (category R, class m) have a value of 12.5% for the night-time net storage

324 heat flux (Fig. 4). This results from only two of the possible 16 classes containing data

325 being improved, hence showing that this is detrimental to predicting the flux.

326

327 The results of Figure 4 show that for some classes (e.g., infinite reflections; category

328 R, class I, Table 4), there are some demonstrated improvements to a flux (e.g., LW_{up})

329 which is not obviously explained by the physics (e.g., how do infinite reflections of

330 shortwave radiation improve the outgoing long-wave radiation but not the reflected
331 shortwave?). Also, there are some classes that improve one particular flux, but not
332 other fluxes. For example, models that represent the net storage heat flux as the
333 residual of the surface energy balance (category S, class r, Table 4) demonstrate a
334 clear improvement for the day-time sensible heat flux, but not for the latent or the net
335 storage heat fluxes. This could be because with such models the sensible heat flux is
336 not constrained by the energy balance giving them the freedom to enable better
337 predictions of the sensible heat flux, whilst moisture availability is still the main
338 control for the latent heat flux.

339

340 There are many such conclusions that can be drawn from Figure 4. Here the focus is
341 on results that are consistent between the fluxes, or consistent for a particular flux
342 between the day-time and night-time.

343

344 Models with a bulk representation of the albedo and emissivity (category A_E, class 1,
345 Table 4), and a bulk representation of facets and orientation (category F_O, class 1; the
346 models in these two classes were identical), demonstrate an improvement in skill
347 during the day-time for nearly all fluxes, with the exceptions of the outgoing long-
348 wave radiation which shows little change in skill and net all-wave radiation fluxes
349 with only small improvements (Fig. 4). This class of models also shows an
350 improvement in the night-time sensible and latent heat fluxes, but degradation in the
351 radiative fluxes during the night. These improved results are most likely due to the
352 ability to utilize the observed bulk albedo directly. This class of models clearly
353 delivers the largest benefits across the fluxes and indicates the most significant
354 physical process to represent is the bulk albedo for the urban surface, because the net

355 shortwave radiation dominates the surface energy balance.

356

357 Improvements to the outgoing long-wave radiation flux and the net all-wave radiation
358 flux during both day-time and night-time are obtained from models that have a single
359 layer for each element of the urban environment (i.e., roofs and either urban canyons,
360 or walls and roads separately) in the morphology category (category L, class 2, Table
361 4; Fig. 4). Improvements to the night-time sensible heat flux and net storage heat flux
362 are also obtained from this class of models, but there is no improvement to these
363 fluxes during the day-time. This neutral day-time result in the sensible and net storage
364 heat fluxes may be explained by the negative impact on the outgoing shortwave
365 radiation flux, which dominates over the long-wave radiation flux during the day-
366 time. However, these results demonstrate the importance of presenting the difference
367 in radiative surface temperatures between the roofs and the urban canyon, due to the
368 non-linear relationship between the upward long-wave radiation and the radiative
369 temperature.

370

371 When considering the way in which the models represent vegetation (category V,
372 Table 4), we find that although including vegetation (classes s and i, Table 4) does
373 generally lead to an improvement for the fluxes, these improvements are not as
374 obvious as those from the bulk albedo or the single layer urban morphology. Hence
375 although these results confirm those presented in earlier studies on the comparison
376 (*Grimmond et al.*, 2011, *Best and Grimmond*, 2013, 2014), that representing
377 vegetation gives improved results, we demonstrate that the more robust analysis
378 presented here shows that this is not the most important physical process as was
379 concluded in these earlier studies. Getting the radiative fluxes correct from the

380 shortwave via the bulk albedo and the long-wave through the urban morphology are
381 required before the vegetation can influence the partitioning of energy between the
382 sensible and latent heat fluxes.

383

384 Previous studies on the urban comparison data have also concluded that models which
385 neglect the anthropogenic heat flux (Q_F) do at least as well as the models that include
386 this flux, although they were unable to explain this result (*Grimmond et al.*, 2011,
387 *Best and Grimmond*, 2013, 2014). However, the results in Figure 4 show that
388 although the class of models that neglect the anthropogenic heat flux (category A_N ,
389 class n, Table 4) do improve some of the fluxes, the improvements are not consistent
390 over all of the fluxes. Moreover, this class of models within the anthropogenic heat
391 flux category is not always the one that delivers the best results. Hence we can
392 conclude that although the models that neglect the anthropogenic heat flux do show
393 some improved results, we cannot make any significant statements about the classes
394 within this category.

395

396 4. Conclusions

397 Prior conclusions from the ULSM comparison with daily (24 h) and seasonal analysis
398 include that: representation of vegetation is critical to model performance (*Grimmond*
399 *et al.*, 2011, *Best and Grimmond*, 2013), along with the associated initial soil moisture
400 (*Best and Grimmond*, 2014), and the bulk albedo is also important (*Grimmond et al.*,
401 2011). Notably, neglecting the distinctive urban anthropogenic heat flux was not
402 found to penalize performance (albeit in the suburban area the value is small) (*Best*
403 *and Grimmond*, 2013). However, this new analysis considering diurnal performance
404 (day, night) enables us to conclude that nocturnal radiative processes also benefit from

405 accounting for the enhanced long-wave trapping that occurs within urban areas.
406 Separating the radiative processes of the roof and the urban canyon is beneficial.
407
408 More critically, the more robust analysis presented here enables identification of a re-
409 prioritisation of the key physical processes: firstly, ensuring the use of the correct bulk
410 albedo for the urban surface; secondly, the outgoing long-wave radiative fluxes with
411 the representation of morphology separated into roofs and urban canyons; and thirdly,
412 the inclusion of vegetation. The implications of the bulk albedo is important for
413 observations as the temporal resolution of satellite estimates mean they will not
414 provide the variations by time of day that are observed (e.g., Christen and Voogt,
415 2004, Grimmond et al. 2004, Kotthaus and Grimmond 2014).

416
417 The current results for anthropogenic heat flux are consistent with the earlier studies:
418 that neglect of the relatively small magnitude flux at this site (study period mean =
419 $\sim 17 \text{ W m}^{-2}$) is reasonable. This conclusion could well be different for urban
420 environments where this is a more significant term in the surface energy balance. The
421 flux is expected to be larger in other areas of Melbourne (e.g., as suggested from
422 analysis using the model of Lindberg et al. 2013) and for urban areas elsewhere. We
423 therefore recommend that future model comparisons ideally include areas of cities
424 with larger anthropogenic heat fluxes.

425
426 Thus to answer the three over-arching research questions of the urban model
427 comparison:
428 (i) The dominant physical processes in the urban environment that models need to be
429 able to simulate, in order, are; changes to the bulk albedo of the surface that result

430 from building materials and also shortwave trapping from the canyon geometry; the
431 reduction in outgoing long-wave radiation from the street canyon due to a reduced
432 sky view factor and the contrast between this and the roofs that see a full sky view;
433 and the evaporation from vegetation.

434 (ii) For the current generation of ULSMs, the ability to utilize a bulk surface
435 albedo (category A_E , class 1, Table 4) and to be able to distinguish between the
436 roofs of buildings and the urban canyons (category L, class 2), and to have a
437 representation of vegetation (category V, classes s, i), results in the best
438 performance.

439 (iii) The key parameters for ULSMs are the bulk surface albedo (information given
440 for Stage 4 influencing the upward shortwave radiation flux), the height to width
441 ratio of the urban canyons and the fraction of building roofs to the urban canyons
442 (information given for Stage 3 influencing the upward long-wave radiation flux),
443 and the vegetation fraction (information given for Stage 2 influencing the sensible
444 and latent heat fluxes).

445

446 The results, from this and the previous studies on the ULSM comparison, all suggest
447 that a simple representation for most of the physical categories is sufficient for this
448 type of application, i.e., determination of local scale fluxes (e.g. for use in the
449 coupling to an atmospheric model). The prior categorization of the models
450 (Grimmond et al., 2011, Best and Grimmond, 2013) into (simple, medium and
451 complex) complexity classes based upon the number of physical categories treated as
452 simple by a model demonstrated that the simple models performed best. This relative
453 success of simple models suggests that for simulating local scale fluxes, more
454 complex schemes deliver little additional benefit. Furthermore, the reduced parameter

455 requirements for simple schemes are advantageous for large scale applications, such
456 as global or regional scale modelling. However, it cannot be expected that this
457 conclusion would also hold for other applications, e.g., atmospheric dispersion within
458 street canyons of a specific city, as the simple models do not present some of the basic
459 physical requirements for such applications. Thus the requirement for the
460 development of more complex ULSMs does remain.

461

462 The implications of this study go beyond the urban environment. In general, we need
463 to balance the requirement for complexity within models against what is actually
464 required for a model to be fit for purpose. Hence new and more complex processes
465 should not be included in models unless it can be demonstrated that they are required.
466 In addition, consideration needs to be given to the availability of information to
467 specify parameters within complex models, and if such complexity can be justified
468 given the uncertainty range for the parameters. Also, the type of analysis used here
469 could be applied to any comparison study to ensure that the results are robust and not
470 contaminated by physical processes not being directly considered.

471

472 These key conclusions are based on the single site observational dataset of less than
473 18 months. This suburban site of low density housing, is typical of extensive areas in
474 North America, Europe and Australasia. Hence we might expect the results from this
475 study to be valid over a reasonable range of cities. However, most urban environments
476 have a range of zones (e.g. *Ellefsen*, 1991, *Grimmond and Souch*, 1994, *Stewart and*
477 *Oke*, 2012) with very different characteristics. So to test if the results presented here
478 are robust for other cities, similar “experiments” are required for additional sites with

479 differing climates and urban characteristics. Hence we recommend that further model
480 comparison projects are required for the urban community.

481

482 Despite these limitations, the results have implications for future development of
483 ULSMs and for the types of data that need to be collected in future urban
484 measurement campaigns (e.g., soil moisture, given its impact to limit transpiration and
485 the long timescales required for model spin-up, along with the conclusion that the
486 fraction of vegetation is important for urban areas) and/or the parameters that should
487 be collated systematically for cities around the world (e.g., *Ching et al.*, 2009, *Loridan*
488 *and Grimmond*, 2012, *Stewart and Oke*, 2012, *Ching*, 2013, *Faroux et al.*, 2013).

489

490 **Acknowledgements** Funds to support the comparison project were provided by the
491 Met Office (P001550). M. Best was supported by the Joint DECC/Defra Met Office
492 Hadley Centre Climate Programme (CA01101). We would like to thank Andrew
493 Coutts and Jason Beringer for allowing their data to be used for the comparison. We
494 would also like to thank Mathew Blackett for all of his efforts in coordinating the
495 model data collection, and to everyone who contributed results to the comparison
496 from their models: J.-J. Baik, S.E. Belcher, J. Beringer, S.I. Bohnenstengel, I. Calmet,
497 F. Chen, A. Dandou, K. Fortuniak, M.L. Gouvea, R. Hamdi, M. Hendry, M. Kanda,
498 T. Kawai, Y. Kawamoto, H. Kondo, E.S. Krayenhoff, S.-H. Lee, T. Loridan, A.
499 Martilli, V. Masson, S. Miao, K. Oleson, R. Ooka, G. Pigeon, A. Porson, Y.-H. Ryu,
500 F. Salamanca, G.J. Steeneveld, M. Tombrou, J.A. Voogt, D.T. Young and N. Zhang.

501

502

503

504 **References**

505

506 Best, M.J. (2005), Representing urban areas within operational numerical weather
507 prediction models. *Boundary-Layer Meteorol*, 114: 91–109.

508 Best M.J., C.S.B. Grimmond, M.G. Villani (2006), Evaluation of the urban tile in
509 MOSES using surface energy balance observations. *Boundary- Layer Meteorol*,
510 118: 503–525.

511 Best M.J., M. Pryor , D.B. Clark, G.G. Rooney, R.H.L. Essery, C.B. Ménard, J.M.
512 Edwards, M.A. Hendry, A. Porson, N. Gedney, L.M. Mercado, S. Sitch, E. Blyth,
513 O. Boucher, P.M. Cox, C.S.B. Grimmond, R.J. Harding (2011) The Joint UK Land
514 Environment Simulator (JULES), Model description – Part 1: Energy and water
515 fluxes. *Geosci Model Dev*, 4: 677-699

516 Best, M.J., C.S.B. Grimmond (2013), Analysis of the seasonal cycle within the first
517 international urban land surface model comparison, *Boundary-Layer Meteorol.*,
518 146, 421-446, doi: 10.1007/s10546-012-9769-7.

519 Best, M.J., C.S.B. Grimmond (2014), Importance of initial state and atmospheric
520 conditions for urban land surface models performance, *Urban Climate*. In press,
521 doi:10.1016/j.uclim.2013.10.006

522 Bohnenstengel, S.I., S. Evans, P.A. Clark, S.E. Belcher (2011), Simulations of the
523 London urban heat island, *Q. J. R. Meteorol. Soc.*, 137, 1625-1640, doi:
524 10.1002/qj.855.

525 Bornstein, R., Q. Lin (2000), Urban heat islands and summertime convection
526 thunderstorms in Atlanta: three case studies, *Atmos. Environ.*, 34, 507-516,
527 doi:10.1016/S1352-2310(99)00374-X.

528 Brunner, D., G. Lemoire, L. Bruzzone, H. Greidonus (2010), Building height retrieval
529 from VHR SAR imagery based on an iterative simulation and matching technique.
530 *IEEE Transactions on Geoscience and Remote Sensing*, 48, No.3,
531 doi:10.1109/TGRS.2009.2031910.

532 Chaxel, E., J.-P. Chollet (2009), Ozone production from Grenoble city during the
533 August 2003 heat wave, *Atmos. Environ.*, 43, 4784-4792,
534 doi:10.1016/j.atmosenv.2008.10.054.

535 Chen F., H. Kusaka, M. Tewari, J. Bao, H. Hirakuchi (2004), Utilizing the coupled
536 WRF/LSM/Urban modeling system with detailed urban classification to simulate
537 the urban heat island phenomena over the Greater Houston area. *Fifth Symposium*
538 *on the Urban Environment*, CD-ROM. 9.11. Amer. Meteor. Soc., Vancouver, BC,
539 Canada.

540 Ching, J.K.S. (2013), A perspective on urban canopy layer modelling for weather,
541 climate and air quality applications, *Urban Climate*, 3, 13-39.

542 Ching, J., M. Brown, S. Burian, F. Chen, R. Cionco, A. Hanna, T. Hultgren, T.
543 McPherson, D. Sailor, H. Taha, D. Williams (2009), National urban database and
544 access portal tool, *Bull. American Meteorol. Soc.*, 90, 1157-1168,
545 doi:10.1175/2009BAMS2675.1.

546 Christen, A., R. Voogt (2004), Energy and radiation balance of a central European
547 city, *Int. J. Climatol.*, 24, 1395-1421, doi:10.1002/joc.1074.

548 Coutts, A.M., J. Beringer, N.J. Tapper (2007a), Characteristics influencing the
549 variability of urban CO₂ fluxes in Melbourne, Australia, *Atmos. Environ.*, 41, 51-
550 62.

551 Coutts, A.M., J. Beringer, N.J. Tapper (2007b) Impact of increasing urban density on
552 local climate: spatial and temporal variations in the surface energy balance in
553 Melbourne, Australia, *J. Appl. Meteorol.*, 47, 477-493.

554 Dandou A., M. Tombrou, E. Akylas, N. Soulakellis, E. Bossioli (2005), Development
555 and evaluation of an urban parameterization scheme in the Penn State/NCAR
556 Mesoscale model (MM5). *J Geophys Res*, 110: D10102.
557 doi:10.1029/2004JD005192.

558 Dupont S., P.G. Mestayer (2006), Parameterisation of the urban energy budget with
559 the submesoscale soil model. *J Appl Meteorol Climatol*, 45: 1744–1765.

560 Dupont S., P.G. Mestayer, E. Guilloteau, E. Berthier, H. Andrieu (2006),
561 Parameterisation of the urban water budget with the submesoscale soil model. *J*
562 *Appl Meteorol Climatol*, 45: 624–648.

563 Ellefsen, R. (1991), Mapping and measuring buildings in the canopy boundary layer
564 in ten U.S. cities. *Energy and Buildings*, 16, 1025-1049.

565 Essery R.L.H., M.J. Best, R.A. Betts, P.M. Cox, C.M. Taylor (2003), Explicit
566 representation of subgrid heterogeneity in a GCM land surface scheme. *J*
567 *Hydrometeorol*, 4: 530–543.

568 Faroux, S., A. T. Kaptue Tchunte, J.-L. Roujean, V. Masson, E. Martin, P. Le
569 Moigne (2013), ECOCLIMAP-II/Europe: a twofold database of ecosystems and
570 surface parameters at 1 km resolution based on satellite information for use in land
571 surface, meteorological and climate models, *Geosci. Model Dev.*, 6, 563-582,
572 doi:10.5194/gmd-6-563-2013.

573 Fortuniak, K. (2003), A slab surface energy balance model (SUEB) and its application
574 to the study on the role of roughness length in forming an urban heat island. *Acta*
575 *Universitatis Wratislaviensis*, 2542, 368-377.

576 Fortuniak K., B. Offerle, C.S.B. Grimmond (2004), Slab surface energy balance
577 scheme and its application to parameterisation of the energy fluxes on urban areas.
578 *NATO ASI, Kiev, Ukraine*; 82–83. Available from: [www.met.rdg.ac.uk/urban](http://www.met.rdg.ac.uk/urban/met/NATO%20ASI/talks.html)
579 [met/NATO ASI/talks.html](http://www.met.rdg.ac.uk/urban/met/NATO%20ASI/talks.html) (Last accessed 4–15 May 2010).

580 Fortuniak K., B. Offerle, C.S.B. Grimmond (2005), Application of a slab surface
581 energy balance model to determine surface parameters for urban areas. *Lund*
582 *Electronic Reports in Physical Geography*, 5: 90–91.

583 Francis, R.A., M.A. Chadwick. (2013), *Urban Ecosystems: Understanding the Human*
584 *Environment. Routledge*, 220pp.

585 Goodwin, N.R., N.C. Coops, T.R. Tooke, A. Christen, J.A. Voogt (2009),
586 Characterizing urban surface cover and structure with airborne lidar technology.
587 *Can. J. Remote Sens.*, 35, 297-309.

588 Grimmond, C.S.B., C. Souch (1994), Surface description for urban climate studies: a
589 GIS based methodology. *Geocarto. International*, 9, 47-59.

590 Grimmond C.S.B., T.R. Oke (2002), Turbulent heat fluxes in urban areas:
591 observations and local-scale urban meteorological parameterization scheme
592 (LUMPS). *J Appl Meteorol*, 41: 792–810.

593 Grimmond, C.S.B., J.A. Salmond, T.R. Oke, B. Offerle, A. Lemonsu (2004), Flux and
594 turbulence measurements at a densely built-up site in Marseille: Heat, mass (water
595 and carbon dioxide), and momentum. *J. Geophys. Res. Atmos.*, 109, D24101,
596 doi:10.1029/2004jd004936

597 Grimmond, C.S.B., M. Blackett, M.J. Best, J. Barlow, J.-J. Baik, S.E. Belcher, S.I.
598 Bohnenstengel, I. Calmet, F. Chen, A. Dandou, K. Fortuniak, M.L. Gouvea , R.
599 Hamdi, M. Hendry, T. Kawai, Y. Kawamoto, H. Kondo, E.S. Krayenhoff, S.-H.
600 Lee, T. Loridan, A. Martilli, V. Masson, S. Miao, K. Oleson, G. Pigeon, A.

601 Porson, Y.-H. Ryu, F. Salamanca, L. Shashua-Bar, G.-J. Steeneveld, M. Trombou,
602 J. Voogt, D. Young, N. Zhang (2010), The international urban energy balance
603 models comparison project: first results from phase 1, *J. Appl. Meteorol.*
604 *Climatol.*, 49, 1268-1292, doi: 10.1175/2010JAMC2354.1.

605 Grimmond, C.S.B., M. Blackett, M.J. Best, J.-J. Baik, S.E. Belcher, J. Beringer, S.I.
606 Bohnenstengel, I. Calmet, F. Chen, A. Coutts, A. Dandou, K. Fortuniak, M.L.
607 Gouvea , R. Hamdi, M. Hendry, M. Kanda, T. Kawai, Y. Kawamoto, H. Kondo,
608 E.S. Krayenhoff, S.-H. Lee, T. Loridan, A. Martilli, V. Masson, S. Miao, K.
609 Oleson, R. Ooka, G. Pigeon, A. Porson, Y.-H. Ryu, F. Salamanca, G.-J.
610 Steeneveld, M. Trombou, J. Voogt, D. Young, N. Zhang (2011), Initial results
611 from phase 2 of the international urban energy balance model comparison, *Int. J.*
612 *Climatol.*, 30, 244-272, doi:10.1002/joc.2227.

613 Hamdi, R., V. Masson (2008), Inclusion of a drag approach in the Town Energy
614 Balance (TEB) scheme: offline 1-D evaluation in a street canyon, *J. Appl.*
615 *Meteorol. Climatol.*, 47, 2627-2644.

616 Harman I.N., M.J. Best, S.E. Belcher (2004a), Radiative exchange in an urban street
617 canyon. *Boundary-Layer Meteorol*, 110: 301–316.

618 Harman I.N., J.F. Barlow, S.E. Belcher (2004b), Scalar fluxes from urban street
619 canyons. Part II: model. *Boundary-Layer Meteorol*, 113: 387–410.

620 Harman I.N., S.E. Belcher (2006), The surface energy balance and boundary layer
621 over urban street canyons. *Q J R Meteorol Soc*, 132: 2749–2768.

622 Herbst, J., K. Mason, R.W. Byard, J.D. Bilbert, C. Charlwood, K.J. Heath, C.
623 Winskog, N.E.I. Langlois (2014), Heat-related deaths in Adelaide, South Australia:
624 Review of the literature and case findings – An Australian perspective, *J. Forensic*
625 *and Legal Medicine*, 22, 73-78. doi:10.1016/j.jflm.2013.12.018

626 Hollinger, D.Y., A.D. Richardson (2005), Uncertainty in eddy covariance
627 measurements and its application to physiological models, *Tree Physiol.*, 25, 873-
628 885.

629 IPCC (2014), Working Group I Contribution to the IPCC Fifth Assessment Report
630 (AR5), Climate Change 2013: The Physical Science Basis. *Intergovernmental*
631 *Panel on Climate Change*, Geneva, Switzerland.

632 Kanda M., T. Kawai, M. Kanega, R. Moriwaki, K. Narita, A. Hagishima (2005a), A
633 simple energy balance model for regular building arrays. *Boundary-Layer*
634 *Meteorol.*, 116: 423–443.

635 Kanda M., T. Kawai, K. Nakagawa (2005b), A simple theoretical radiation scheme
636 for regular building arrays. *Boundary-Layer Meteorol.*, 114: 71–90.

637 Kawai T., M. Kanda, K. Narita, A. Hagishima (2007), Validation of a numerical
638 model for urban energy-exchange using outdoor scalemodel measurements. *Int J*
639 *Climatol.*, 27: 1931–1942.

640 Kawai T., M.K. Ridwan, M. Kanda (2009), Evaluation of the simple urban energy
641 balance model using 1-yr flux observations at two cities. *J Appl Meteorol Climatol.*
642 48: 693–715.

643 Kawamoto Y., R. Ooka (2006), Analysis of the radiation field at pedestrian level
644 using a meso-scale meteorological model incorporating the urban canopy model. In
645 *ICUC-6, Göteborg, Sweden*, 12–16 June 2006.

646 Kawamoto Y., R. Ooka (2009a), Accuracy validation of urban climate analysis model
647 using MM5 incorporating a multi-layer urban canopy model. In *ICUC-7,*
648 *Yokohama, Japan*, 28 June–3 July 2009.

649 Kawamoto Y., R. Ooka (2009b) Development of urban climate analysis model using
650 MM5 Part 2 – incorporating an urban canopy model to represent the effect of
651 buildings. *J Environ Eng* (Transactions of AIJ) 74(642): 1009–1018 (in Japanese).

652 Kondo H., F.H. Liu (1998), A study on the urban thermal environment obtained
653 through a one-dimensional urban canopy model, *J Jpn Soc Atmos Environ.* 33,
654 179-192 (in Japanese)

655 Kondo H., Y. Genchi, Y. Kikegawa, Y. Ohashi, H. Yoshikado, H. Komiyama (2005),
656 Development of a multi-layer urban canopy model for the analysis of energy
657 consumption in a big city: structure of the urban canopy model and its basic
658 performance. *Boundary-Layer Meteorol.*, 116: 395–421.

659 Kotthaus, S., C.S.B. Grimmond (2013), Energy exchange in a dense urban
660 environment - Part II: Impact of spatial heterogeneity of the surface, *Urban
661 Climate*, [hppt://dx.doi.org/10.1016/j.uclim.2013.10.001](https://doi.org/10.1016/j.uclim.2013.10.001).

662 Krayenhoff, E.S., J.A. Voogt (2007), A microscale three-dimensional urban energy
663 balance model for studying surface temperatures, *Boundary-Layer Meteorol.*, 123,
664 433-461.

665 Kusaka, H., H. Kondo, Y. Kikegawa, F. Kimura (2001), A simple singlelayer urban
666 canopy model for atmospheric models: comparison with multi-layer and slab
667 models, *Boundary-Layer Meteorol.*, 101, 329-358.

668 Laaidi, K., A. Zeghnoun, B. Dousset, P. Bretin, S. Vandentorren, E. Giraudet, P.
669 Beaudeau (2012), The impact of heat islands on mortality in Paris during the
670 August 2003 heat wave, *Environ. Health Perspectives*, 120, 254-259,
671 [doi:10.1289/ehp.1103532](https://doi.org/10.1289/ehp.1103532).

672 Lee, S.-H., S.-U. Park (2008), A vegetated urban canopy model for meteorological
673 and environmental modelling, *Boundary-Layer Meteorol.*, 126, 73-102.

674 Lemonsu A., C.S.B. Grimmond, V. Masson (2004), Modelling the surface energy
675 balance of an old Mediterranean city core. *J Appl Meteorol*, 43: 312–327.

676 Li, C.B., J.J. Zhou, Y.J. Cao, J. Zhong, Y. Liu, C.Q. Kang, Y. Tan (2014), Interaction
677 between urban microclimate and electric air-conditioning energy consumption
678 during high temperature season, *Applied Energy*, 117, 149-156,
679 doi:10.1016/j.apenergy.2013.11.057.

680 Lindberg, F., C.S.B. Grimmond (2011), Nature of vegetation and building
681 morphology characteristics across a city: Influence on shadow patterns and mean
682 radiant temperatures in London. *Urban Ecosyst.*, 14, 617-623. doi:10.1007/s11252-
683 011-0184-5.

684 Lindberg, F., C.S.B. Grimmond, N. Yogeswaran, S. Kotthaus, L. Alen (2013),
685 Impacts of city changes and weather on anthropogenic heat flux in Europe 1995-
686 2015, *Urban Climate*, 4, 1-15. <http://dx.doi.org/10.1016/j.uclim.2013.03.002>.

687 Loridan T., C.S.B. Grimmond, S. Grossman-Clarke, F. Chen, M. Tewari, K.
688 Manning, A. Martilli, H Kusaka, M. Best (2010), Trade-offs and responsiveness of
689 the single-layer urban canopy parameterization in WRF: an offline evaluation
690 using the MOSCEM optimization algorithm and field observations. *Q J R Meteorol*
691 *Soc*, 136: 997–1019. doi:10.1002/qj.614.

692 Loridan T., C.S.B. Grimmond, B.D. Offerle, D.T. Young, T. Smith, L. Järvi, F.
693 Lindberg (2011), Local-scale urban meteorological parameterization scheme
694 (LUMPS): Longwave radiation parameterization and seasonality-related
695 developments. *J Appl Meteorol Climatol*, 50: 185-202.
696 doi:10.1175/2010JAMC2474.1

697 Loridan, T., C.S.B. Grimmond (2012), Multi-site evaluation of an urban land-surface
698 model: intra-urban heterogeneity, seasonality, and parameter complexity
699 requirements. *Q. J. R. Meteorol. Soc.*, 138, 1094-1113, doi:10.1002/qj.963.

700 Luhar, A.K., M. Thatcher, P.J. Hurley (2014) Evaluating a building-averaged urban
701 surface scheme in an operational mesoscale model for flow and dispersion, *Atmos.*
702 *Environ.*, 88, 47-58, doi:10.1016/j.atmosenv.2014.01.059.

703 Martilli A., A. Clappier, M.W. Rotach (2002), An urban surface exchange
704 parameterisation for mesoscale models. *Boundary-Layer Meteorol*, 104: 261–304.

705 Masson V. (2000) A physically-based scheme for the urban energy budget in
706 atmospheric models. *Boundary-Layer Meteorol*, 41: 1011–1026.

707 Masson V., C.S.B. Grimmond, T.R. Oke (2002), Evaluation of the Town Energy
708 Balance (TEB) scheme with direct measurements from dry districts in two cities. *J*
709 *Appl Meteorol*, 41: 1011–1026.

710 McCarthy, M.P., M.J. Best, R.A. Betts (2010), Climate change in cities due to global
711 warming and urban effects, *Geophys. Res. Letters*, 37, L09705,
712 doi:10.1029/2010GL042845.

713 Offerle B., C.S.B. Grimmond, T.R. Oke (2003), Parameterization of net all-wave
714 radiation for urban areas. *J Appl Meteorol*, 42: 1157–1173.

715 Oke TR (2006) Towards better scientific communication in urban climate. *Theor.*
716 *Appl. Climatol.* 84: 179-190. doi: 10.1007/s00704-005-0153-0

717 Oleson, K.W., G.B. Bonan, J. Feddema, M. Vertenstein, C.S.B. Grimmond (2008a),
718 An urban parameterization for a global climate model: 1. Formulation and
719 evaluation for two cities, *J. Appl. Meteorol. Climatol.*, 47, 1038-1060.

720 Oleson K.W., G.B. Bonan, J. Feddema, M. Vertenstein. 2008b. An urban
721 parameterization for a global climate model: 2. Sensitivity to input parameters and

722 the simulated heat island in offline simulations. *J Appl Meteorol Climatol*, 47:
723 1061–1076.

724 Oleson, K.W., G.B. Bonan, J. Feddema, T. Jackson (2011), An examination of urban
725 heat island characteristics in a global climate model, *Int. J. Climatol.*, 31, 1848-
726 1865. doi:10.1002/joc.2201.

727 Pickett, S.T.A., M.L. Cadenasso, J.M. Grove, P.M. Groffman, L.E. Band, C.G. Boone,
728 W.R. Burch, Jr., C.S.B. Grimmond, J. Hom, J.C. Jenkins, N.L. Law, C.H. Nilon,
729 R.V. Pouyat, K. Szlavecz, P.S. Warren, M.A. Wilson. 2008. Beyond urban
730 legends: an emerging framework of urban ecology, as illustrated by the Baltimore
731 Ecosystem Study. *BioScience*. 58(2):139-150

732 Pigeon G., M.A. Moscicki, J.A. Voogt, V. Masson (2008), Simulation of fall and
733 winter surface energy balance over a dense urban area using the TEB scheme.
734 *Meteorol Atmos Phys*, 102: 159–171.

735 Porson A., P.A. Clark, I.N. Harman, M.J. Best, S.E. Belcher (2010), Implementation
736 of a new urban energy budget scheme in the MetUM. Part II. Validation against
737 observations and model intercomparison. *Q J R Meteorol Soc*, 136: 1530-1542.

738 Radhi, H., S. Sharples (2013), Quantifying the domestic electricity consumption for
739 air-conditioning due to urban heat islands in hot arid regions, *Applied Energy*, 112,
740 371-380, doi:10.1016/j.apenergy.2013.06.013.

741 Ryu Y.-H., J.-J. Baik, S.-H. Lee (2011), A new single-layer urban canopy model for
742 use in mesoscale atmospheric models. *J Appl Meteorol Climatol*, 50: 1773-1794.
743 doi: 10.1175/2011JAMC2665.1

744 Ryu, Y.-H., J.J. Baik (2013), Effects of anthropogenic heat on ozone air quality in a
745 megacity. *Atmos. Environ.*, 80, 20-30, doi:10.1016/j.atmosenv.2013.07.053.

746 Saha, M.V., R.E. Davis, D.M. Hondula (2014), Mortality displacement as a function
747 of heat event strength in 7 US cities, *American J. Epidemiology*, 179, 467-474,
748 doi:10.1093/aje/kwt264.

749 Sailor, D.J., L. Lu (2004), A top-down methodology for developing diurnal and
750 seasonal anthropogenic heating profiles for urban areas. *Atmos. Environ.*, 38,
751 2737-2748, doi:10.1016/j.atmosenv.2004.01.034.

752 Salamanca F., E.S. Krayenhoff, A. Martilli (2009), On the derivation of material
753 thermal properties representative of heterogeneous urban neighbourhoods. *J Appl*
754 *Meteorol Climatol*, 48: 1725–1732.

755 Salamanca F., A. Krpo, A. Martilli, A. Clappier (2010), A new building energy model
756 coupled with an urban canopy parameterization for urban climate simulations –
757 part I. Formulation, verification, and sensitivity analysis of the model. *Theor Appl*
758 *Climatol*, 99: 345-356. doi: 10.1007/s00704-009-0142-9.

759 Salamanca F., A. Martilli (2010), A new Building Energy Model coupled with an
760 Urban Canopy Parameterization for urban climate simulations – part II. Validation
761 with one dimension off-line simulations. *Theor Appl Climatol*, 99: 345–356.

762 Sarrat, C., A. Lemonsu, V. Masson, D. Guedalla (2006), Impact of urban heat island
763 on regional atmospheric pollution, *Atmos. Environ.*, 40, 1743-1758,
764 doi:10.1016/j.atmosenv.2005.11.037.

765 Stewart, I.D., T.R. Oke (2012), Local climate zones for urban temperature studies,
766 *Bull. American Meteorol. Soc.*, 93, 1879-1900, doi:10.1175/BAMS-D-11-00019.1.

767

768 **Figure captions**

769 Figure 1: Conceptual figure of how surface energy balance exchanges are included in
770 urban land surface models of different complexity. Note individual models have
771 simple and complex features (Grimmond et al., 2011).

772

773 Figure 2: For each flux and physical category class (Table 4), the percentage of
774 modelled data points within the specified observational errors (eqn. 1) for Stages 1
775 and 4 (grey) plus the change relative to the previous stage (eqn. 2; scaled between -
776 100% and 100%, shown by the horizontal dotted lines). Blue shading indicates an
777 improvement (> 0) and red degradation (< 0). Results are shown for day and night-
778 time (with day defined as incoming solar radiation flux greater than 0 W m^{-2}). Codes
779 definition for the physical categories and component classes (used in the x-axis) are
780 given in Table 4

781

782 Figure 3: As for Fig. 2, but for the radiative fluxes

783

784 Figure 4: The subset of models within a class of a category improved compared to all
785 models (P_{ca} , eqn. 4) ranked according to the median over the stages (for each flux, by
786 time of day (as for Fig. 2)). Shading shows the range of results over the stages, with
787 the individual results shown as horizontal lines within this. The colouring emphasises
788 the values of the median over the stages, with 100% corresponding to all classes
789 improved, 0% all classes degraded and 50% no change. Note X-axis code (Table 4)
790 order changes between subplots because of ranking (Colour text is to aid differences
791 to be noted).

792

793

794 **Table 1:** Urban land surface models (ULSMs) used to obtain results that are analysed
795 here. See Grimmond et al. (2010, 2011) for more details of the different model
796 versions and the number of groups that submitted simulations to the urban model
797 comparison.
798

Model name	References
Building effect parameterization (BEP)	Martilli et al. (2002) Salamanca et al. (2009, 2010) ; Salamanca and Martilli (2010)
Community Land Model – urban (CLM-urban)	Oleson et al. (2008a, 2008b)
Institute of Industrial Science urban canopy model	Kawamoto and Ooka (2006, 2009a, 2009b)
Joint UK land environment simulator (JULES)	Essery et al. (2003); Best (2005); Best et al. (2006); Best et al. (2011)
Local-scale urban meteorological parameterization scheme (LUMPS)	Grimmond and Oke (2002); Offerle et al. (2003); Loridan et al. (2011)
Met Office Reading urban surface exchange scheme (MORUSES)	Harman et al. (2004a, 2004b); Harman and Belcher (2006), Porson et al. (2010)
Multi-layer urban canopy model	Kondo and Liu (1998); Kondo et al. (2005)
National and Kapodistrian University of Athens model	Dandou et al. (2005)
Noah land surface model/single-layer urban canopy model	Kusaka et al. (2001); Chen et al. (2004); Loridan et al. (2010)
Seoul National University urban canopy model	Ryu et al. (2011)
Simple urban energy balance model for mesoscale simulation	Kanda et al. (2005a, 2005b); Kawai et al. (2007, 2009)
Slab urban energy balance model	Fortuniak (2003); Fortuniak et al. (2004, 2005)
Soil model for submesoscales (urbanized)	Duport and Mestayer (2006); Dupont et al. (2006)
Temperatures of urban facets (TUF)	Krayenhoff and Voogt (2007)
Town energy balance (TEB)	Masson (2000); Masson et al. (2002); Lemonsu et al. (2004); Pigeon et al. (2008), Hamdi and Masson (2008)
Vegetated urban canopy model	Lee and Park (2008)

799

800 Table 2: Methods used to obtain the observed fluxes used for comparison with the
 801 ULSM. Sources: *Coutts et al.*, (2007a, 2007b). Height of observation for all fluxes: 40
 802 m.
 803

Flux	Instrument / Method	Sampling frequency (Hz.)	Averaging period (min)
SW_{up} LW_{up} Q^*	Kipp and Zonen CM7B and CG4 radiometers	1	30
Q_H	CSI CSAT 3D sonic anemometer	10	30
Q_E	CSI CSAT 3D sonic anemometer CSI Krypton hygrometer (Aug 2003 – Feb 2004), LiCOR LI7500 open-path infrared gas analyser (remaining period)	10	30
ΔQ_S	Residual of the surface energy balance	N/A	30
Q_F	Calculated (<i>Sailor and Lu</i> , 2004) : <i>Vehicles</i> : Numbers from survey (Nov. 2002 – Oct 2003) <i>Building sector</i> : 30 min electricity and daily natural gas statistics <i>Human metabolism</i> : Night, day and transition period metabolic rates, with population density statistics	N/A	Average monthly diurnal cycle at 30 min. resolution

804

805

806 Table 3. Information released at each stage of the comparison

Stage	Information released
1	Atmospheric forcing data only (incoming shortwave radiation, incoming long-wave radiation, precipitation, atmospheric wind speed, temperature, specific humidity and surface pressure)
2	Vegetation and built fractions
3	Morphology (Building heights, height-to-width ratio, mean wall to plan area ratio, fraction of surface covered by buildings, concrete, road,)
4	Specific information on building materials (e.g., albedo and thermal properties of wall, road, roof)
5	Observed fluxes for parameter optimisation (Not considered in this study)

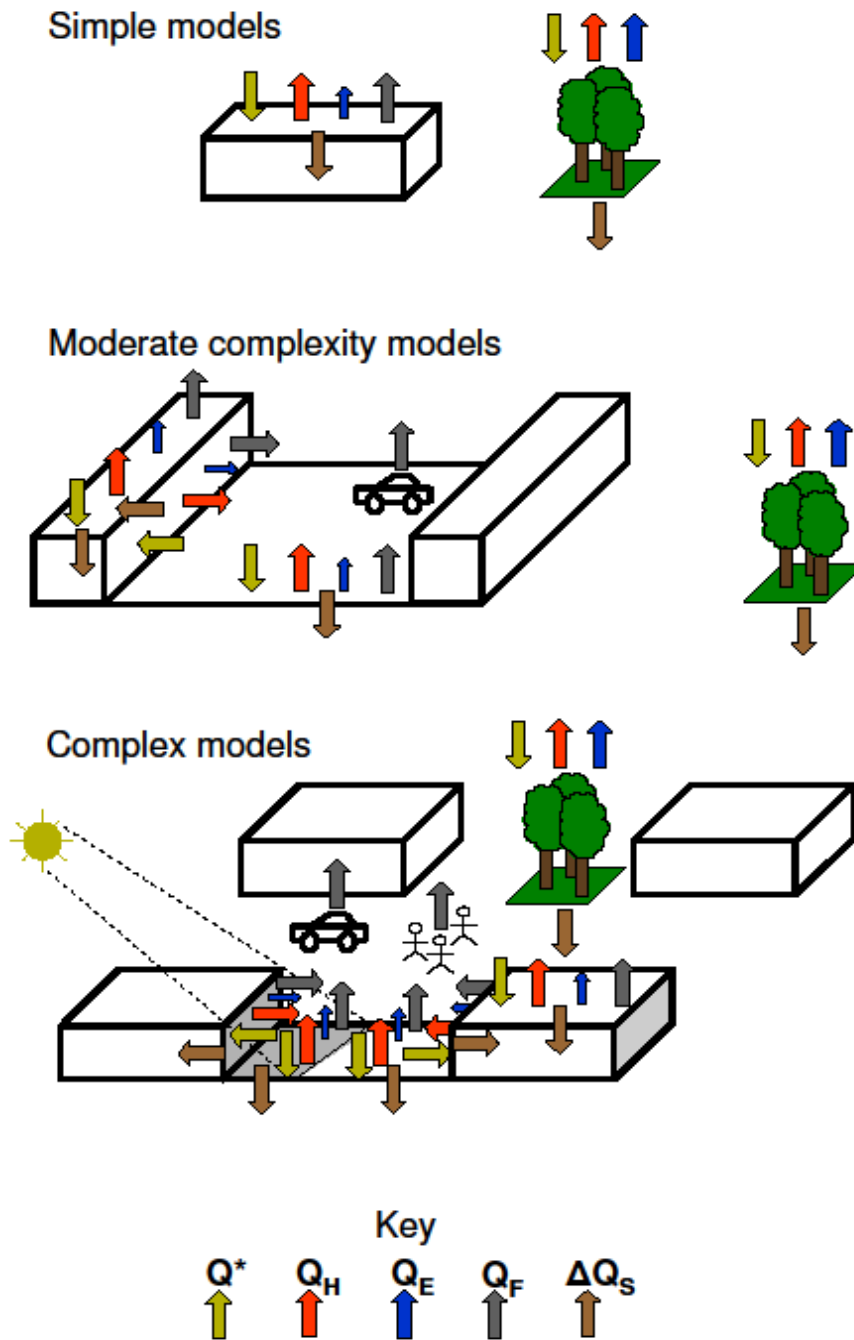
807

808 Table 4: Classes and physical categories used in the analysis of the urban comparison
809 results, including the number of models in each class (see *Grimmond et al.*, 2010,
810 2011 for more details). Colours are used on the plots to aid comparison.

Category	Class			
Vegetation (V)	None (n)	Separate tile (s)	Integrated (i)	
No. of models	8	19	5	
Anthropogenic heat flux (A_N)	None (n)	Prescribed flux (p)	Internal building temperature (i)	Modelled (m)
No. of models	22	2	6	2
Temporal variation of the anthropogenic heat flux (T)	None (i.e., no flux) (n)	Fixed (i.e., time invariant flux) (f)	Variable (i.e., time varying flux) (v)	
No. of models	22	3	7	
Urban morphology (L)	Bulk (1)	Single layer (2)	Multiple layer (4)	
No. of models	6	20	6	
Facets & orientation (F_o)	Bulk (1)	Roof, walls, road without orientation (n)	Roof, walls, road with orientation, no intersections (o)	Roof, walls, road with orientation and intersections (i)
No. of models	5	17	6	4
Reflections (R)	Single (1)	Multiple (m)	Infinite (i)	
No. of models	11	13	8	
Albedo, emissivity (A_E)	Bulk (1)	Two facet (2)	Three facet (3)	
No. of models	5	4	23	
Net storage heat flux (S)	Net all wave radiation (n)	Surface energy balance residual (r)	Conduction equation (c)	
No. of models	3	6	23	

811

812



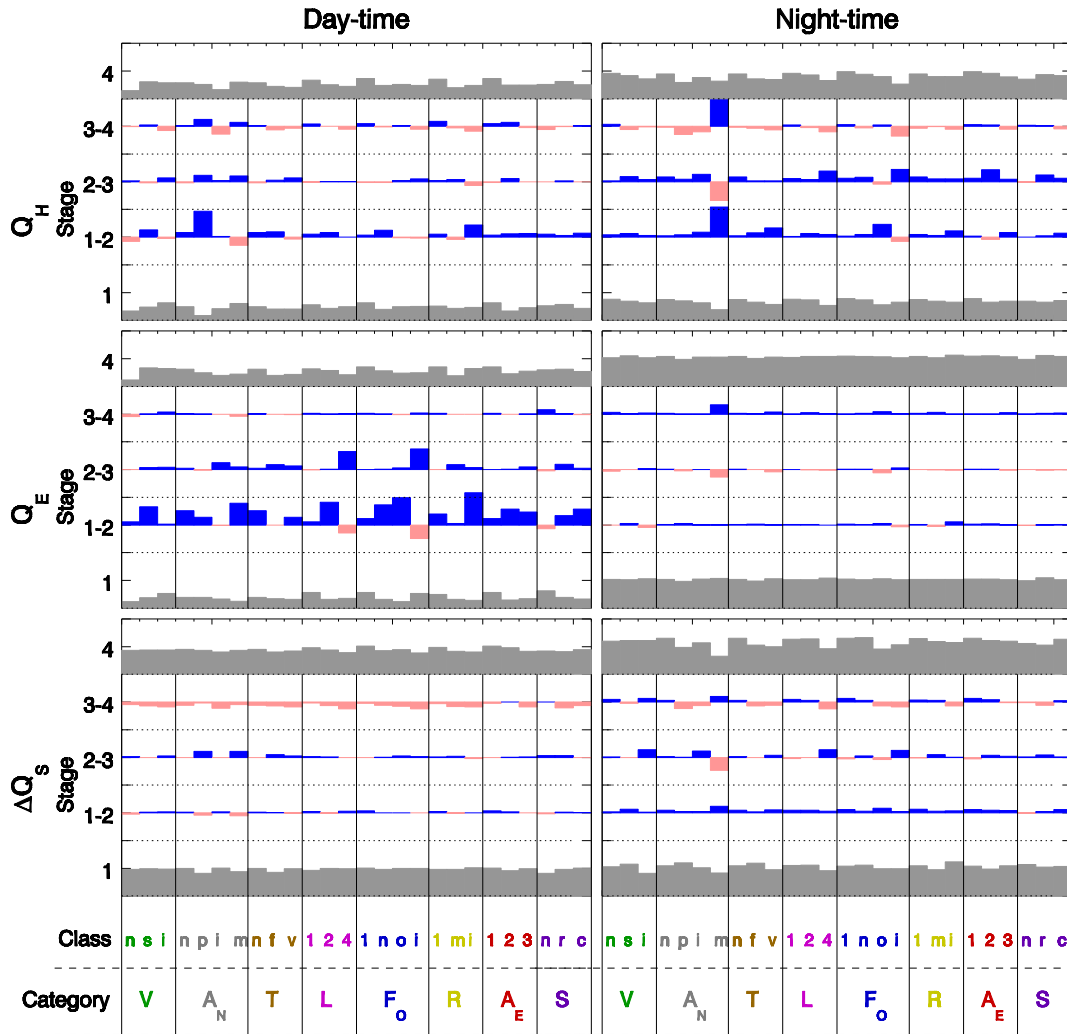
813

814 Figure 1: Conceptual figure of how surface energy balance exchanges are included in

815 urban land surface models of different complexity. Note individual models have

816 simple and complex features (Grimmond et al., 2011).

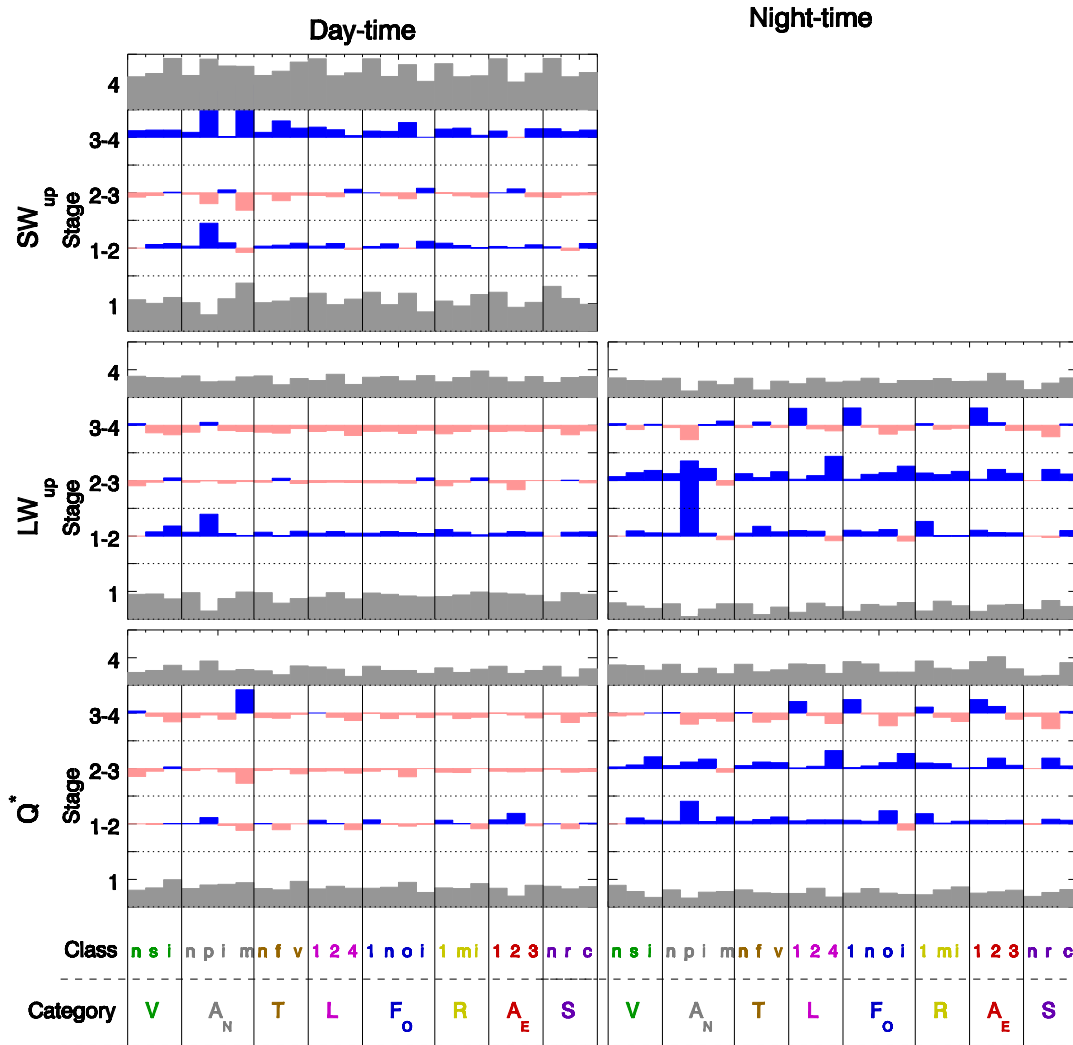
817



818

819 Figure 2: For each flux and physical category class (Table 4), the percentage of
 820 modelled data points within the specified observational errors (eqn. 1) for Stages 1
 821 and 4 (grey) plus the change relative to the previous stage (eqn. 2; scaled between
 822 -100% and 100%, shown by the horizontal dotted lines). Blue shading indicates an
 823 improvement (> 0) and red degradation (< 0). Results are shown for day and
 824 night-time (with day defined as incoming solar radiation flux greater than 0 W m^{-2}).
 825 Codes definition for the physical categories and component classes (used in the
 826 x-axis) are given in Table 4.

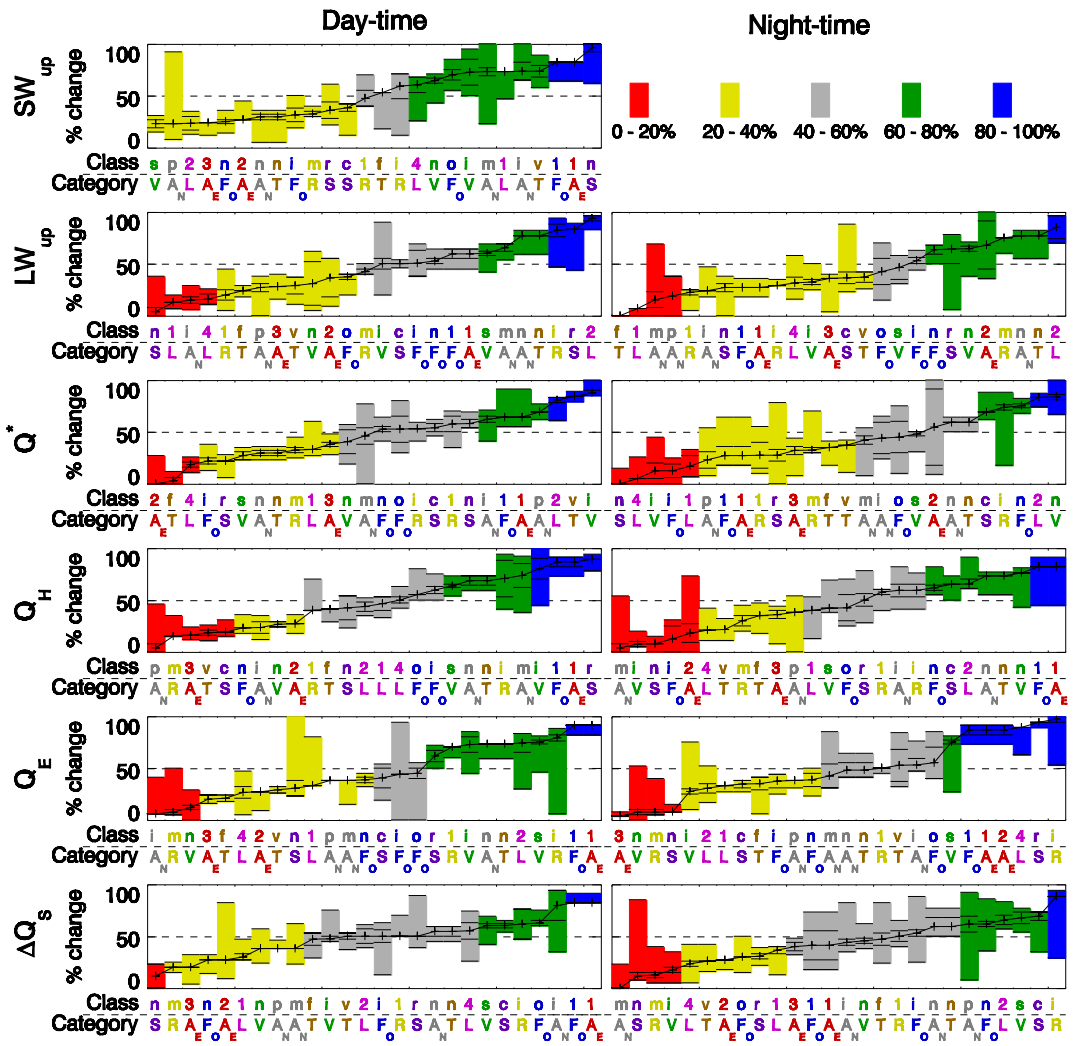
827



828

829 Figure 3: As for Fig. 2, but for the radiative fluxes.

830



831

832 Figure 4: The subset of models within a class of a category improved compared to all
 833 models (P_{ca} , eqn. 4) ranked according to the median over the stages (for each flux,
 834 by time of day (as for Fig. 2)). Shading shows the range of results over the stages,
 835 with the individual results shown as horizontal lines within this. The colouring
 836 emphasises the values of the median over the stages, with 100% corresponding to
 837 all classes improved, 0% all classes degraded and 50% no change. Note X-axis
 838 code (Table 4) order changes between subplots because of ranking (Colour text is
 839 to aid differences to be noted).

840